Available online at www.sciencedirect.com
ScienceDirect
Trans. Nonferrous Met. Soc. China 25(2015) 3072−3079
Transactions of Nonferrous Metals Society of China
www.tnmsc.cn

Determination of local constitutive behavior and simulation on tensile test of 2219-T87 aluminum alloy GTAW joints

Yan-jun LI[1,2,3], Quan LI[1,2,3], Ai-ping WU[1,2,3], Ning-xu MA[4], Guo-qing WANG[5], Hidekazu MURAKAWA[4], Dong-yang YAN[5], Hui-qiang WU[5]

1. Department of Mechanical Engineering, Tsinghua University, Beijing 100084, China;
2. State Key Laboratory of Tribology, Tsinghua University, Beijing 100084, China;
3. Key Laboratory for Advanced Materials Processing Technology, Ministry of Education, Tsinghua University, Beijing 100084, China;
4. Joining and Welding Research Institute, Osaka University, Osaka, Ibaraki 567-0047, Japan;
5. China Academy of Launch Vehicle Technology, Beijing 100076, China

Received 8 October 2014; accepted 11 April 2015

Abstract: The local and global mechanical responses of gas tungsten arc welds (GTAW) of a 2219-T87 aluminum alloy were investigated with experiment and numerical simulation. Digital image correlation (DIC) was used to access the local strain fields in transversely loaded welds and to determine the local stress−strain curves of various regions in the joint. The results show that the DIC method is efficient to acquire the local stress−strain curves but the curves of harder regions are incomplete because the stress and strain ranges are limited by the weakest region. With appropriate extrapolation, the complete local stress−strain curves were acquired and proved to be effective to predict the tensile behavior of the welded joint. During the tensile process, the fracture initiates from the weld toes owing to their plastic strain concentrations and then propagates along the fusion line, finally propagates into the partially melted zone (PMZ).

Key words: aluminum alloy; tensile behavior; digital image correlation; constitutive behavior; welded joint

1 Introduction

2219-T87 aluminum alloy has excellent cryogenic properties, high fracture toughness and stress corrosion resistance. It is widely used in manufacturing of fuel tanks for large launch vehicles, such as Thor-Deta, Saturn-II, space shuttle [1−3] and supersonic craft [4]. Variable polarity gas tungsten arc welding (GTAW) has been proved as an appropriate process for welding aluminum alloys and has a widespread application in industries, especially in aviation and aerospace.

The service behavior and the strength of the 2219-T87 GTAW joint are complicated and mainly affected by three reasons. 1) The stress concentration around the weld toes needs to be considered when weld reinforcement is applied. 2) The partially melted zone (PMZ) adjacent to the weld deteriorates the ductility of the GTAW joint due to the continuous grain boundary θ phase formed during welding [5−7]. 3) The over-aged zone has poor strength which is adjacent to PMZ. Until now, the microstructure and strength evolution in aluminum alloy hardened by precipitate during a welding process has been studied largely and well understood [8−12]. However, the effects of the local material properties and geometric sizes of sub-regions on the overall loading behavior of the inhomogeneous high strength aluminum alloy GTAW joint are still not fully understood [13−15]. Numerical simulation is an efficient way to link the local properties in various regions to the macroscopic response and to predict the mechanical behavior of the joint having complex gradient microstructure [16−18]. However, the accuracy of the simulation depends on the accurate local material properties for various zones of the welded joint. Several methods have been developed for acquiring local material properties of the inhomogeneous welds, including hardness testing across the welds [8,19,20],

Foundation item: Project (2012 2X04012-011) supported by the Innovation Platform for Process Modeling and Simulation of Advanced Materials Processing Technologies, China
Corresponding author: Yan-jun LI; Tel: +86-10-62773859-5; Fax: +86-10-62773859-5; E-mail: liyanjun12@mails.tsinghua.edu.cn
DOI: 10.1016/S1003-6326(15)63935-8

testing of micro-specimens [15,21], testing of thermally simulated materials [22] and a combination of tensile test and digital image correlation (DIC) [23].

Digital image correlation (DIC) as a non-contacting strain measurement method is frequently used to determine the local constitutive properties of heterogeneous materials, especially welded joints [16,17,24,25]. By assuming the iso-stress condition during the loading of transverse tensile specimen, the local stress−strain curves are acquired by mapping the applied stress and the local strain via DIC. The DIC technique overcomes many limitations and shortcomings of the previously mentioned methods, but it exhibits one limitation that strain mapping allows to obtain the complete stress−strain curves only in the weakest region [16].

In this work, 2219-T87 aluminum alloy plates with 6 mm in thickness were butt-welded by conducting single-sided two-pass GTAW process. Various tensile tests of the joints with or without weld reinforcement were conducted to record the load-deformation process and to investigate the tensile behavior of the joints. The complete constitutive behaviors in various zones of the joint were determined and verified by comparing the tensile responses obtained by testing transverse weld with those obtained by numerical simulation. The tensile behavior of the joint was investigated with experiment and numerical simulation.

2 Experimental

The base material was the 2219 aluminum alloy plate under T87 heat treatment condition with dimensions of 300 mm × 150 mm × 6.0 mm. The nominal chemical composition is shown in Table 1. The filler metal was ER2319 with a diameter of 1.6 mm, and its nominal chemical composition is also shown in Table 1. The butt joint was fulfilled with single-sided two-pass welding process. The first pass adopted direct current (DC) GTAW process without groove and filler metal, and the second pass adopted variable polarity-pulsed current (VP-PC) GTAW process with filler metal of ER2319. The welding parameters used are listed in Table 2.

The specimen used for hardness testing was cut from the joint perpendicular to the direction of welding. The specimen was suitably mounted, ground with different grades of emery papers and polished using diamond pastes. After polishing, the specimen was etched in Keller’s reagent (2 mL HF + 3 mL HCl + 5 mL HNO_3 + 190 mL H_2O) for 15−25 s. The micro-hardness tests were conducted along the straight lines across the weld at an interval of 0.5 mm using MH−3 type micro-hardness tester with a load of 1 N and a holding time of 10 s. The hardness locations are illustrated schematically in Fig. 1. The bottom line is in the first welding pass and the upper one is in the second welding pass.

Table 1 Chemical compositions of 2219 and ER2319 filler material

Alloy	Mass fraction/%				
	Si	Fe	Cu	Mn	Mg
2219	0.2	0.3	5.8−6.8	0.2−0.4	0.02
ER2319	0.2	0.3	5.8−6.8	0.2−0.4	0.02
Alloy	Mass fraction/%				
	Zn	Ti	Zr	V	Al
2219	0.1	0.02−0.10	0.10−0.25	0.05−0.15	Bal.
ER2319	0.1	0.10−0.20	0.10−0.25	0.05−0.15	Bal.

Table 2 Welding parameters

Parameter	DC GTAW	VP-PC GTAW
Peak current/A	200	300
Base current/A	−	155
Peak voltage/V	19	22
Base voltage/V	−	16
Travel speed/($cm\cdot min^{-1}$)	27	14
Shielding gas	He	Ar
Shielding gas flow rate/($L\cdot min^{-1}$)	10	12
Pulse frequency/Hz	−	0.8
Duty ratio	−	66.7%

The tensile specimens were cross-sectioned perpendicularly to the welding direction. The transverse tensile test of the joint was conducted according to GB/T 228.1−2010 standard with a constant speed of 2 mm/min. The load−displacement curves were recorded. The dimensions of the tensile sample are shown in Fig. 2. The gauge length was 50 mm. The DIC device was Aramis 4M optical measuring system developed by GOM mbH.

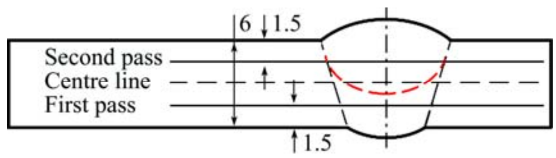

Fig. 1 Location of micro-hardness testing (unit: mm)

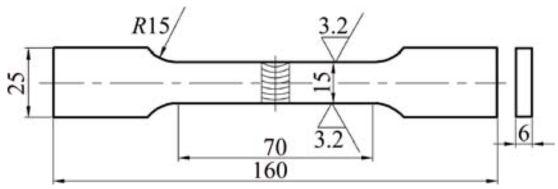

Fig. 2 Dimensions of tensile specimen (unit: mm)

3 Simulation model and verification

3.1 Finite element modeling

With finite element (FE) analysis ABAQUS/CAE v6.10-1 software package, a 3D numerical model was developed to simulate the transverse tensile test of the welded 2219 aluminum alloy sheets. The modelled geometry was in agreement with the specimen used for transverse tensile test. The dimensions of the modelled specimen were the same as those shown in Fig. 2. The measured cross-weld micro-hardness profiles, as shown in Fig. 3, indicate that the mechanical properties vary seriously through the weld. Therefore, the model was based on a composite material approach and the welded joint was divided into several regions in which the properties were assumed to be uniform.

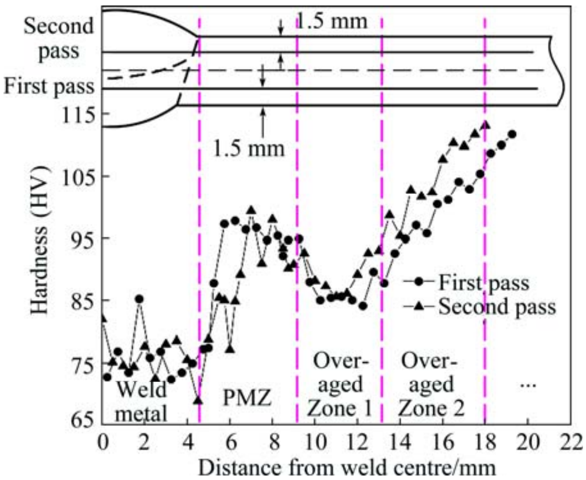

Fig. 3 Distribution of hardness on transverse cross-section

Figure 4 shows the details of the modelled tensile specimen. The modelled specimen is decomposed into 13 regions. The half of the joint includes weld metal, PMZ, four over-aged zones numbered by 1, 2, 3 and 4, and base material. The profiles of different regions were determined according to the hardness values and the

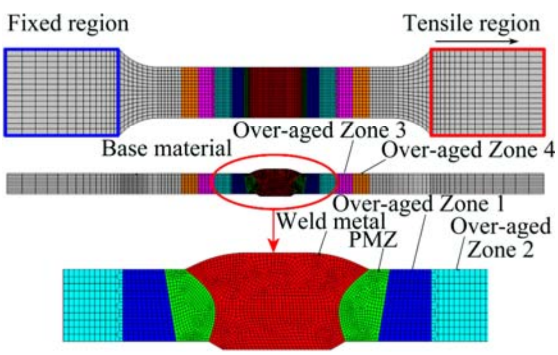

Fig. 4 Numerical simulation model of joint with weld reinforcement

variations of metallographic structure. The finite element discretization used 3D eight-node hexahedron iso-parametric elements. The model consisted of 107834 nodes and 98970 elements. To simulate the tensile process of the welded joint, *x*, *y* and *z* constraints were imposed on the nodes in the fixed region, and a velocity of 2 mm/min in longitudinal direction was applied to the tensile region. During uniaxial tension, the deformation at the given gauge length and the axial force was recorded, and then the load−deformation curve was obtained. The fracture behavior of the joint was modeled using the fracture strain criterion, in which the corresponding element failed as the equivalent plastic strains of the integration points reached their fracture strain.

3.2 Determination of local stress−strain curves

The local true stress−strain curves in each region could be calculated from local strain fields registered with DIC method during tensile tests of transverse weld specimens [25]. With the local strain values acquired using DIC method, the evolution of the cross sectional area of a specific part in the specimen can be calculated using the following relationship:

$$A = A_{\mathrm{o}} \exp(-\varepsilon) \tag{1}$$

where A and A_{o} are the actual and initial cross sectional areas of the part of specimen, and ε is the local axial true strain. Then, the local stress in this area can be obtained by dividing the applied load, F, by the actual cross sectional area, A. At this point, the local stress−strain curves can be determined. However, the complete tensile response could hardly be obtained by DIC because of strain localization and necking. The complete tensile response is important for the accuracy of numerical simulation, so extrapolation method must be developed to complete the tensile response of different zones.

With the DIC technique, the incomplete true stress−strain curves of the weld metal, PMZ and over-aged Zone 1 were obtained. The fracture strains $\varepsilon_{\mathrm{f}}^{\mathrm{p}}$ of these zones were calculated according Eq. (2) as follows:

$$\varepsilon_{\mathrm{f}}^{\mathrm{p}} = \sqrt{\frac{2}{3}\varepsilon_{ij}^{\mathrm{p}}\varepsilon_{ji}^{\mathrm{p}}} = \sqrt{\frac{2}{3}[(\varepsilon_{xx}^{\mathrm{p}})^2 + (\varepsilon_{yy}^{\mathrm{p}})^2 + (\varepsilon_{zz}^{\mathrm{p}})^2]} \tag{2}$$

where $\varepsilon_{yy}^{\mathrm{p}} = \ln\left(\frac{b}{b_{\mathrm{o}}}\right)$, $\varepsilon_{zz}^{\mathrm{p}} = \ln\left(\frac{t}{t_{\mathrm{o}}}\right)$, $\varepsilon_{xx}^{\mathrm{p}} = -(\varepsilon_{yy}^{\mathrm{p}} + \varepsilon_{zz}^{\mathrm{p}})$ $= \ln\left(\frac{b_{\mathrm{o}}t_{\mathrm{o}}}{bt}\right)$, b_{o}, t_{o} and A_{o} are the initial width, thickness and area of the transverse section of the specimen, respectively, b, t and A are the width, thickness and area of the fractured section, respectively.

In order to extrapolate the plastic behavior up to the fracture strain from the incomplete tensile stress−strain curve, Eq. (3) was adjusted to the incomplete curves. The fitted material parameters are presented in Table 3 and the complete true stress−strain curves, plotted according to experimental results and Eq. (3), are shown in Fig. 5 (DIC and Model 1). The first half of the stress−strain curves, indicated by solid lines, were plotted according to experimental results while the extrapolated part, indicated by dash dot lines, were plotted according to Eq. (3).

$$\sigma = k\varepsilon^n = \sigma_o \left(\frac{\varepsilon}{\varepsilon_o}\right)^n \tag{3}$$

where σ_o is the linear elastic limit of the true stress−strain curve, ε_o is the strain corresponding to the linear elastic limit, n is the strain hardening exponent.

The parameters of the over-aged Zones 2, 3, 4 were linearly interpolated by Eq. (4) using the material parameters of base material and over-aged Zone 1.

$$\begin{cases} \sigma_{oi} = \sigma_{o1} + \dfrac{i-1}{4}(\sigma_{oBM} - \sigma_{o1}) \\ n_{oi} = n_{o1} + \dfrac{i-1}{4}(n_{oBM} - n_{o1}) \end{cases}, \ i=2,3,4 \tag{4}$$

where σ_{oi} and n_{oi} are the linear elastic limit and the hardening exponent of the over-aged Zone i (i=1, 2, 3, 4), respectively. σ_{oBM} and n_{oBM} are the linear elastic limit and the hardening exponent of the base material, respectively.

Table 3 Material parameters of various areas in joint

Area	Linear elastic limit, σ_o/MPa	Hardening exponent, n	Fracture strain, ε_f^p	Maximum stress of Model 1/MPa	Maximum stress of Model 2/MPa
Weld metal	73	0.31	0.22	392	335
PMZ	110	0.30	0.16	450	398
Over-aged Zone 1	90	0.31	0.32	503	415
Over-aged Zone 2	155	0.26	0.31	565	446
Over-aged Zone 3	220	0.21	0.31	585	477
Over-aged Zone 4	285	0.16	0.31	576	507
Base material	349	0.11	0.31	605	538

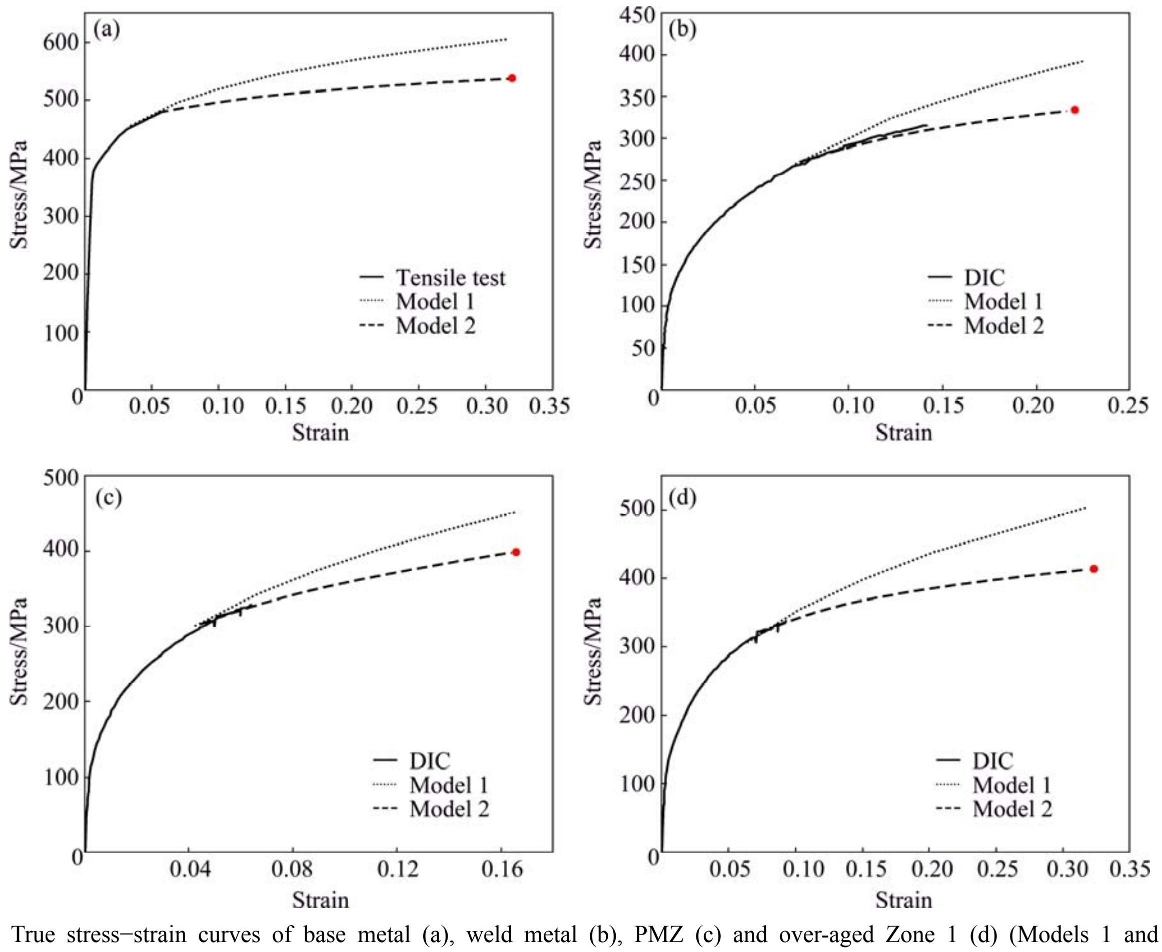

Fig. 5 True stress−strain curves of base metal (a), weld metal (b), PMZ (c) and over-aged Zone 1 (d) (Models 1 and 2 are extrapolated by Eq. (2) and maximum points, respectively)

The elastic modulus and Poisson's ratio of different regions were set as uniform value (E=73.1 GPa and μ=0.33). In the FE model, as shown in Fig.4, the left side of the specimen was fixed and the load was applied to the right side. During the uniaxial tensile test, the deformation at the given gauge length and the axial force was recorded and then the load−deformation curve was obtained. The computed load−deformation curves of the base material and the joint without weld reinforcement was compared with the test results (Fig. 6). The first half of the computed curves agrees very well with the experimental curves, whereas after yielding and before necking, the computed curve seriously deviates from the experimental result. This is because the extrapolated curves obtained by Eq. (3) are not accurate. Therefore, a more appropriate extrapolation method should be developed.

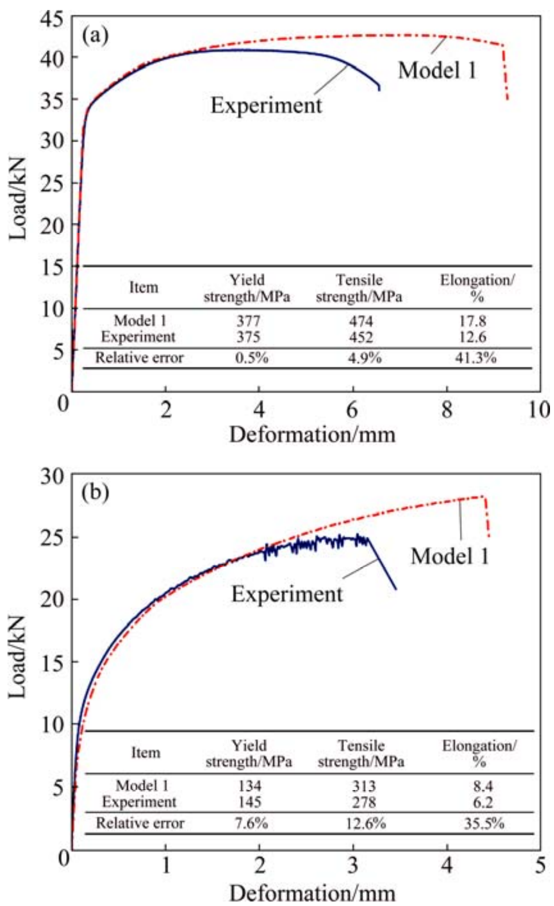

Fig. 6 Load−deformation curves of base material (a) and joint without weld reinforcement (b) calculated by Model 1

The maximum true stress of the weld, PMZ, over-aged Zone 1 and base metal can be deduced from the fracture loads and the fractured cross-sections in the corresponding zones. The calculated maximum true stresses are shown in Table 3 and indicated by the red dots in Fig. 5. To extrapolate the complete tensile responses, the incomplete true stress−strain curves were extended smoothly to the maximum points, as shown in Fig. 5 (Model 2). With the complete true stress−strain curves obtained by Model 2, the tensile simulations of the base metal and the joint without weld reinforcement were computed again. As shown in Fig. 7, the computed results show a good agreement with the experimental results. For the joint without weld reinforcement, the yield stress, tensile strength and elongation are all consistent with the experimental results, and the slight discrepancies are 7.6%, 1.1% and 0.3%, respectively. The joint fractures at the middle of the weld zone both in the simulation and tensile test, as shown in Fig. 8. The good agreement between experimental and computed results indicates that the extrapolation method in Model 2 works well in deducting the complete tensile response.

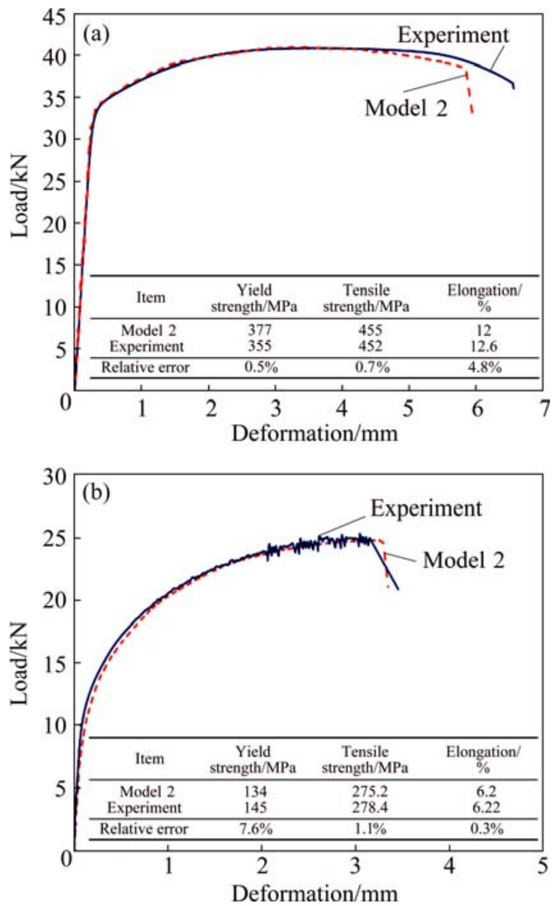

Fig. 7 Load−deformation curves of base material (a) and joint without weld reinforcement (b) calculated by Model 2

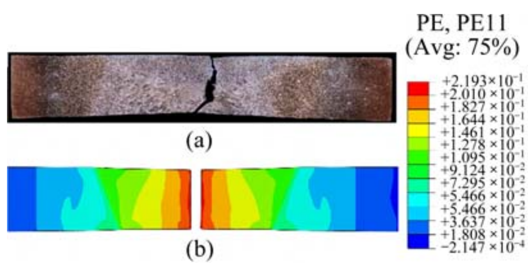

Fig. 8 Fractured joints without reinforcements: (a) Experiment; (b) Simulation

4 Tensile behavior of as-welded joint

With the simulation model developed and verified above, the tensile behavior of the as-welded joint was investigated by simulation. The variation of the equivalent plastic strain and equivalent stress distributions on the central cross-section of the joints are shown in Fig. 9. During the tensile process, the weld metal around the weld toes yields first (Figs. 9(a) and (b)), then the PMZ around the weld toes yields, and finally the over-aged Zone 1 yields (Figs. 9(c) and (d)). The strain concentration around the weld toes is observed in the model, which is located both in the weld metal and PMZ. In simulation, the fracture initiated from the weld toes (Figs. 9(e) and (f)) owing to the strain concentration, then propagated along the fusion line, and finally into the PMZ (Fig. 10(a)). In the real tensile test, the joint shows the same fracture path as the simulation result (Fig. 10(b)). The stress in the weld metal is lower than that in the PMZ due to the effect of the weld reinforcement (the stress concentrations around the weld toes).

The distributions of strain ε_{xx} obtained by simulation and DIC test are shown in Fig. 11. It can be found that the strain distribution, the maximum strain location, and the strain values of the simulation and DIC results are in good agreement. The weld metal and PMZ around the weld toes endure a serious strain (about 16%) and the over-aged Zone 1 also withstands a large tensile strain (about 10%).

The load−displacement curves obtained from simulation and experiment are shown in Fig. 12. The results of simulation and experiment have a good agreement (the difference is lower than 5%). The superior agreement between the simulation and experiment shows that, the model is capable of predicting accurately the global tensile behavior of 2219 aluminum alloy joints with and without reinforcement.

In comparison, the tensile properties of joints with reinforcement are superior to those of joints without reinforcement. The yield strength and tensile strength of the joint with reinforcement are 15 and 43 MPa, respectively, which are higher than those of joints without reinforcement. The hardness distribution in Fig. 3 indicates that the weld zone has the lowest strength. As the reinforcement increases the effective loading area of the weld zone, the weakest zone is

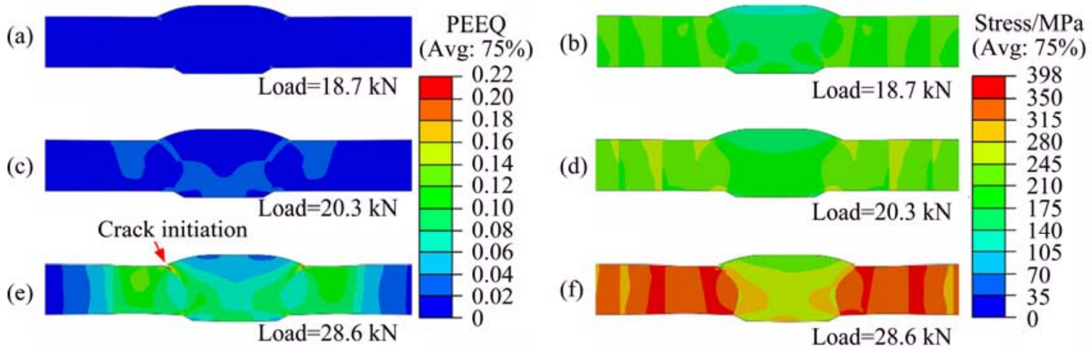

Fig. 9 Distributions of equivalent strain (a, c, e) and stress (b, d, f) on central cross-section of joints during tensile

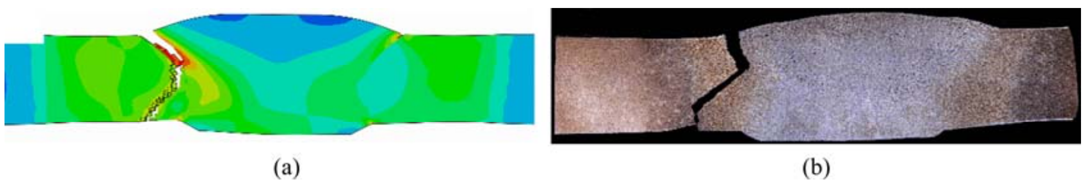

Fig. 10 Fractured joints with reinforcements after tension: (a) Simulation; (b) Experiment

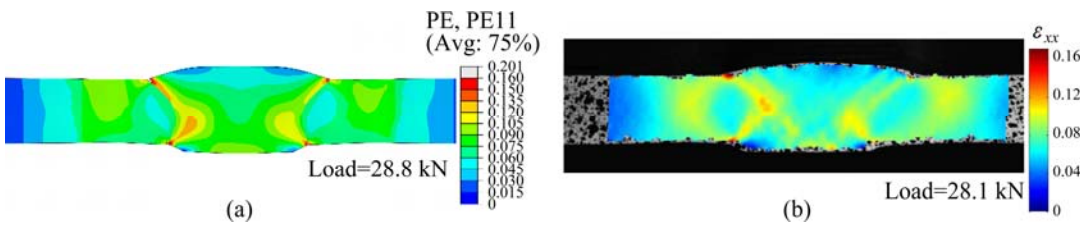

Fig. 11 Distributions of strain ε_{xx} on edge surface corresponding to fracture initiated from simulation (a) and DIC test (b)

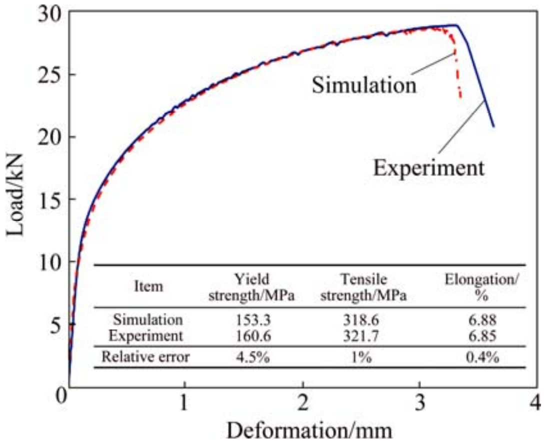

Fig. 12 Load−displacement curves obtained from simulation and experiment

strengthened, and finally the joint strength is improved. In addition, the elongation data reveal that the joint with reinforcement has better ductility.

The present study proves that DIC method is effective to measure the local constitutive properties of heterogeneous joints. The very limitation of DIC method that it is unable to acquire the complete tensile responses of all the zones can be resolved with appropriate extrapolation, as described before. With the complete local stress−strain curves of various zones, the tensile properties of joint can be predicted quantitatively and amend with finite element modeling.

5 Conclusions

1) DIC method is proved to be efficient to obtain the local tensile responses in various zones of 2219-T87 aluminum GTAW joint. One shortcoming of the DIC method is that it can hardly acquire the complete tensile responses due to the strain concentration and necking. The extrapolation method based on the maximum true stress is turned out to be effective to deduce the complete tensile responses. The computed load−deformation curves of the base metal and joints with/without weld reinforcement show a good agreement with the experimental results.

2) During the tensile process, the weld metal around the weld toes yields first, then the PMZ around the weld toes yields, and finally the metals of the over-aged Zone 1 yield. The simulation shows that the fracture initiates from the weld toes owing to their plastic strain concentrations and then propagates along the fusion line, and the final failure is present in the PMZ. The stress in the weld metal is lower than that in the PMZ, due to the effect of weld reinforcement. There are some stress concentrations in the metals around the weld toes. In addition, the reinforcement can improve the strength and ductility of the joint.

References

[1] NARAYANA G V, SHARMA V M J, DIWAKAR V, KUMAR K S, PRASAD R C. Fracture behaviour of aluminium alloy 2219-T87 welded plates [J]. Science and Technology of Welding and Joining, 2004, 9(2): 121−130.

[2] XU Wei-feng, LIU Jin-he, LUAN Guo-hong, DONG Chun-lin. Microstructures and mechanical properties of friction stir welded aluminum alloy thick plate [J]. Acta Metallurgica Sinica, 2008, 44(11): 1404−1408. (in Chinese)

[3] XU Wei-feng, LIU Jin-he, LUAN Guo-hong, DONG Chun-lin. Temperature evolution, microstructure and mechanical properties of friction stir welded thick 2219-O aluminum alloy joints [J]. Materials and Design, 2009, 30(6): 1886−1893.

[4] WANG Zhu-tang, TIAN Rong-zhang. Aluminum alloy and its manufacturing [M]. 2nd ed. Changsha: Central South University Press, 2000. (in Chinese)

[5] HUANG C, KOU S. Partially melted zone in aluminum welds: Solute segregation and mechanical behavior [J]. Welding Journal, 2001, 80(1): 9−17.

[6] HUANG C, KOU S. Partially melted zone in aluminum welds—Liquation mechanism and directional solidification [J]. Welding Journal, 2000, 79(5): 113−120.

[7] RAO K S, REDDY G M, RAO K P. Studies on partially melted zone in aluminium−copper alloy welds—Effect of techniques and prior thermal temper [J]. Materials Science and Engineering A, 2005, 403(1−2): 69−76.

[8] AMBRIZ R R, CHICOT D, BENSEDDIQ N, MESMACQUE G, de la TORRE S D. Local mechanical properties of the 6061-T6 aluminium weld using micro-traction and instrumented indentation [J]. European Journal of Mechanics-A/Solids, 2011, 30(3): 307−315.

[9] DING Ji-kun, WANG Dong-po, WANG Ying, DU Hui. Effect of post weld heat treatment on properties of variable polarity TIG welded AA2219 aluminium alloy joints [J]. Transactions of Nonferrous Metals Society of China, 2014, 24(5): 1307−1316.

[10] MYHR O R, GRONG O, FJAER H G, MARIOARA C D. Modelling of the microstructure and strength evolution in Al−Mg−Si alloys during multistage thermal processing [J]. Acta Materialia, 2004, 52(17): 4997−5008.

[11] RINGER S P, SOFYAN B T, PRASAD K S, QUAN G C. Precipitation reactions in Al−4.0Cu−0.3Mg (wt.%) alloy [J]. Acta Materialia, 2008, 56(9): 2147−2160.

[12] ZANG Jin-zin, ZHANG Kun, DAI Sheng-long. Precipitation behavior and properties of a new high strength Al−Zn−Mg−Cu alloy [J]. Transactions of Nonferrous Metals Society of China, 2012, 22(11): 2638−2644.

[13] GORDON STEPHEN S. An investigation into geometry and microstructural effects upon the ultimate tensile strengths of butt welds [R]. Washington DC: NASA, 1992.

[14] NUNES A C, NOVAK H L, MCILWAIN M C. Weld geometry strength effect in 2219-T87 aluminum [R]. Washington DC: NASA, 1981.

[15] SIMAR A, BRECHET Y, de MEESTER B, DENQUIN A, PARDOEN T. Microstructure, local and global mechanical properties of friction stir welds in aluminium alloy 6005A-T6 [J]. Materials Science and Engineering A, 2008, 486(1−2): 85−95.

[16] GENEVOIS C, DESCHAMPS A, VACHER P. Comparative study on local and global mechanical properties of 2024 T351, 2024 T6 and 5251 O friction stir welds [J]. Materials Science and Engineering A, 2006, 415(1−2): 162−170.

[17] LOCKWOOD W D, REYNOLDS A P. Simulation of the global

response of a friction stir weld using local constitutive behavior [J]. Materials Science and Engineering A, 2003, 339(1−2): 35−42.
[18] PANDA S K, SREENIVASAN N, KUNTZ M L, ZHOU Y. Numerical simulations and experimental results of tensile test behavior of laser butt welded DP980 steels [J]. Journal of Engineering Materials and Technology, 2008, 130(4): 0410034.
[19] IMAM M, BISWAS K, RACHERLA V. Effect of weld morphology on mechanical response and failure of friction stir welds in a naturally aged aluminium alloy [J]. Materials and Design, 2013, 44: 23−34.
[20] LIN J, MA N S, LEI Y P, MURAKAWA H. Investigation of interface layer failure and shear strength of CMT brazed lap joints in dissimilar materials [J]. Transactions of JWRI, 2011, 40(1): 101−107.
[21] RAO D, HUBER K, HEERENS J, dos SANTOS J F, HUBER N. Asymmetric mechanical properties and tensile behaviour prediction of aluminium alloy 5083 friction stir welding joints [J]. Materials Science and Engineering A, 2013, 565: 44−50.
[22] HVAL M, THAULOW C, LANGE J H, HOYDAL S H, ZHANG Z L. Numerical modeling of ductile fracture behavior in aluminum weldments [J]. Welding Journal, 1998, 77(5): 208−217.
[23] REYNOLDS A P, DUVALL F. Digital image correlation for determination of weld and base metal constitutive behavior [J]. Welding Journal, 1999, 78(10): 355−360.
[24] BOYCE B L, REU P L, ROBINO C V. The constitutive behavior of laser welds in 304L stainless steel determined by digital image correlation [J]. Metallurgical and Materials Transactions A, 2006, 37(8): 2481−2492.
[25] LEITAO C, GALVAO I, LEAL R M, RODRIGUES D M. Determination of local constitutive properties of aluminium friction stir welds using digital image correlation [J]. Materials and Design, 2012, 33: 69−74.

2219-T87 铝合金 GTAW 焊接接头的局部本构关系测量及单向拉伸数值模拟

李艳军 [1,2,3]，李 权 [1,2,3]，吴爱萍 [1,2,3]，麻宁绪 [4]，王国庆 [5]，
Hidekazu MURAKAWA [4]，鄢东洋 [5]，吴会强 [5]

1. 清华大学 机械工程系，北京 100084；
2. 清华大学 摩擦学国家重点实验室，北京 100084；
3. 清华大学 先进成形制造教育部重点实验室，北京 100084；
4. Joining and Welding Research Institute, Osaka University, Osaka, Ibaraki 567-0047, Japan；
5. 中国运载火箭技术研究院，北京 100076

摘 要：通过实验和数值模拟方法研究 2219-T87 铝合金钨极氩弧焊接接头(GTAW)的局部及全局力学性能。采用数字图像相关(DIC)技术对拉伸过程的变形进行测量，并获取接头不同区域的局部应力−应变曲线。结果表明：DIC 方法可以有效地测量非均匀接头的局部本构关系，但存在局限性，只有最薄弱区(断裂位置)才能得到完整的应力−应变曲线。通过外延得到了其他区域完整的应力−应变关系，并应用于单向拉伸模拟，模拟结果与实验结果具有良好的一致性，验证了材料本构关系的正确性。在拉伸过程中由于应变集中，裂纹从焊趾启裂，沿着熔合线扩展，最后扩展进入部分熔化区(PMZ)。

关键词：铝合金；拉伸性能；数字图像相关；本构关系；焊接

(Edited by Mu-lan QIN)